

# Dynamics of the $\text{N}(^4S_u) + \text{NO}(X^2\Pi) \rightarrow \text{N}_2(X^1\Sigma_g^+) + \text{O}(^3P_g)$ atmospheric reaction on the $^3A''$ ground potential energy surface. I. Analytical potential energy surface and preliminary quasiclassical trajectory calculations

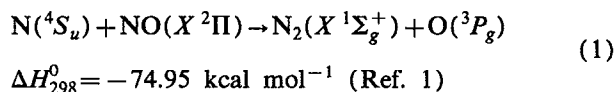
Miquel Gilibert,<sup>a)</sup> Antonio Aguilar, Miguel González, Fernando Mota, and R. Sayós  
Departament de Química Física, Facultat de Química, Universitat de Barcelona Martí i Franquès, 1,  
08028 Barcelona, Spain

(Received 17 April 1992; accepted 22 June 1992)

The  $\text{N}(^4S_u) + \text{NO}(X^2\Pi) \rightarrow \text{N}_2(X^1\Sigma_g^+) + \text{O}(^3P_g)$  reaction plays an important role in the upper atmosphere chemistry and as a calibration system for discharge flow systems. Surprisingly, very little theoretical and experimental work has been devoted to the characterization of the dynamical features of this system. In this work a Sorbie–Murrell expression for the lowest  $^3A''$  potential energy surface (PES) connecting reactants in their ground electronic states based upon the fitting of an accurate *ab initio* CI grid of points has been derived. The PES fitted shows no barrier to reaction with respect to the reactants asymptote in accordance with experimental findings and becomes highly repulsive as the NNO angle is varied away from the saddle point geometry. The results of preliminary quasiclassical trajectory calculations on this surface reproduce very well the experimental energy disposal in products, even though the vibrational distribution derived from trajectories seems to be a bit cooler than the experimental data. Moreover, thermal rate constants derived from trajectories are in excellent accordance with experimental values.

## I. INTRODUCTION

The reaction of nitric oxide with ground state  $\text{N}(^4S_u)$  atoms:



has routinely been used as a means of determining NO concentrations in low pressure discharge flow systems, and has also been employed to determine NO concentrations in combustion exhaust gases. Besides its practical implications, the reactions of nitrogen with nitric oxide are thought to play an important role in the chemistry of the upper atmosphere. In particular, reaction (1) would act as a sink for NO molecules above 40 km.<sup>2,3</sup>

Even though the importance of acquiring a thorough theoretical and experimental knowledge of this kind of systems seems rather justified, relatively little attention has been paid to their characterization.

Experimental work on reaction (1) has been mainly limited to rate constant measurements using different techniques. The first such determination by Kistiakowsky and Volpi<sup>4</sup> using a discharge flow system with mass spectrometric measurement of products gave a lower bound for the absolute rate constant  $k$  at 298 K of  $4.0 \times 10^{11} \text{ cm}^3/\text{mol s}$ . Phillips and Schiff<sup>5</sup> obtained a value of  $(1.3 \pm 0.4) \times 10^{13} \text{ cm}^3/\text{mol s}$  using a fast flow technique. This value coincides with the discharge flow results of Clyne and McDermid,<sup>6</sup> where the temperature dependence of  $k$  between 298 and 670 K is also explored. Even though there is a considerable scatter in the measurements, as the temperature  $T$  increases a final Arrhenius-like dependence

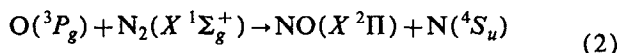
of  $k$  vs  $T$  is deduced  $\{k = (4.9 \pm 0.8) \times 10^{13} \exp[-(410 \pm 120)/T]\} \text{ cm}^3/\text{mol s}$  leading to an estimate of 0.82 kcal/mole for the activation energy. The only other existing temperature dependence study of the rate constant for reaction (1) was determined by Lee *et al.*<sup>7</sup> using resonant fluorescence detection of products. In this work, the flash photolysis and discharge flow techniques were used to derive the behavior of  $k$  with  $T$  between 196–300 K and 233–400 K, respectively. The results obtained clearly disagree with the findings of Clyne and McDermid<sup>6</sup> in that a negative or no dependence of  $k$  on the temperature is observed. Their best estimate for  $k$  in the 196–400 K interval is nevertheless independent of  $T$  [ $(2.0 \pm 0.5) \times 10^{13} \text{ cm}^3/\text{mol s}$ ]. Recent measurements of  $k$  at different temperatures ranging from 1600–2285 K by Koshi *et al.*<sup>8</sup> using resonant atomic absorption led to the conclusion that reaction (1) should proceed with very little or no activation energy. The best value for  $k$  reported by these authors is  $(1.3 \pm 0.3) \times 10^{13} \text{ cm}^3/\text{mol s}$  over the whole energy range studied. There have been other determinations of  $k$  over the years using different experimental techniques.<sup>9–12</sup> Most of these values fall within statistical errors from each other and from the Baulch *et al.*<sup>13</sup> recommended value of  $(1.6 \pm 0.3) \times 10^{13} \text{ cm}^3/\text{mol s}$  at 300 K.

There have been several studies aimed at determining the energy disposal in products for reaction (1). Morgan *et al.*<sup>14,15</sup> evaluated the vibrational energy content of the  $\text{N}_2$  molecules formed using an isothermal calorimeter with mass spectrometric detection of products. These authors used ozone as a probe of the vibrational energy content of products by measuring the fraction of molecules formed with enough vibrational energy to decompose ozone ( $E_{\text{vib}} \geq 24.0 \text{ kcal/mole}$ ). The authors concluded that the fraction of exothermicity going into vibration of products

<sup>a)</sup> Author for correspondence.

is  $0.28 \pm 0.07$  and that  $75\% \pm 5\%$  of the  $N_2$  molecules formed appear in vibrational levels above  $v' = 4$ . Therefore, it is to be expected that the  $N_2$  resulting from reaction (1) will be formed with a non-Maxwellian distribution. Wray *et al.*<sup>16</sup> suggested that the hot  $N_2$  distribution observed in Refs. 14 and 15 could result from collisions of translationally hot oxygen atoms formed in reaction (1) with nitrogen molecules. In a more recent paper, Black *et al.*<sup>17</sup> carried out flow tube experiments with Raman detection of products to estimate the efficiency of the conversion between the exothermicity of the reaction and vibrational energy of products. They find out a value of  $0.25 \pm 0.03$  for the fraction of exothermicity disposed of as vibration of  $N_2$ . Since this value is maintained even for measurements carried out under such conditions that collisional deactivation of hot oxygen atoms by  $N_2$  molecules was very unlikely, it is concluded that the vibrational inversion of products does in fact stem from available energy being channeled into vibration.

The effect of relative energy on the reverse reaction:



$$\Delta H_{298}^0 = 74.95 \text{ kcal mol}^{-1} \text{ (Ref. 1)}$$

has been studied by Wray *et al.*<sup>16</sup> using a shock tube technique. Their experimental results agree well with theoretical calculations in which only the translational energy is employed to overcome the endothermicity of the reaction and seem to rule out the intermediate case in which the sum of translational and vibrational energy can be used to overcome the endothermicity of the reaction. To our knowledge the only existing trajectory study of these reactions has been performed on reaction (2) by Jaffe *et al.*<sup>18</sup> on the  $^3A''$  potential energy surface using a modified LEPS surface including an angle-dependent term to reproduce the ONN angular saddle point. The rate constant results reported in this work show low error margins above 7000 K, even though the authors state that their determinations for temperatures below 2000 K bear large statistical errors. Their theoretical results agree well with the experimental rate constants for reaction (2) in the narrow range of temperatures where they overlap. In this study, they also find out that internal energy favors reaction, in apparent disagreement with Wray *et al.*,<sup>16</sup> but also in accordance with the late character of the barrier on the  $^3A''$  PES for reaction (2).

This paper is organized as follows: in Sec. II a description of the model and the fitting procedure for the potential energy surface employed in the calculations is given, in Sec. III the results of a preliminary quasiclassical trajectory study are reported, and finally in Sec. IV conclusions are drawn.

## II. POTENTIAL ENERGY SURFACE

### A. Characterization of the ground state potential energy surface

The electronic ground state of the  $N(^4S_u) + NO(X^2\Pi)$  reactants adiabatically correlates with prod-

ucts in their ground electronic state [Eq. (1)] through the  $d^3\Pi$  potential energy surface in  $C_{\infty v}$  symmetry. The ground  $X^1\Sigma^+$  state of the  $N_2O$  molecule correlates in  $C_{\infty v}$  symmetry with the  $NO(X^2\Pi) + N(^2D_u)$  and  $O(^1D_g) + N_2(X^1\Sigma_g^+)$  states of reactants and products. On going from  $C_{\infty v}$  to  $C_s$  symmetry, the  $d^3\Pi$  PES gives rise through avoided crossings with the  $a^3\Sigma^+$  and  $b^3\Delta$  surfaces to the lowest lying  $1^3A'$  and  $1^3A''$  surfaces, respectively. Thus in  $C_s$  geometries the ground states of reactants and products become correlated through the two lowest lying triplet surfaces. This agrees with the *ab initio* multireference CI findings of Walch and Jaffe<sup>19</sup> who obtained bent saddle points for both surfaces and highly repulsive behaviors of the bending potentials, with both interatomic distances held constant at their saddle point values, as the angle between the NN and NO bonds is varied away from the saddle point value. These theoretical findings do also agree very well with the experimental data which seem to indicate that reaction (1) should proceed with no or very low activation energy. As a matter of fact, these authors find out a value of 0.5 kcal/mole for the barrier on the lowest  $^3A''$  PES, fully compatible with the experimental error margins for the evaluation of this magnitude. No minima on the  $1^3A'$  and  $1^3A''$  PESs have been reported in the above-mentioned *ab initio* calculations. This is consequent with the theoretical MCSCF/CI calculations of Hopper,<sup>20</sup> who reported values for the  $1^3A'$  and  $1^3A''$  states of the  $N_2O$  molecule above the  $N_2(X^1\Sigma_g^+) + O(^3P_g)$  asymptote.

Even though these MCSCF/CI calculations yield adiabatic transition energies between the different states of  $N_2O$  with an estimated 0.5–1.0 eV error margin, they can be used together with the available spectroscopic data<sup>21–23</sup> to build a qualitative partial correlation diagram (Fig. 1). More information as well as detailed diagrams can be found in Ref. 20.

Figure 2 shows the minimum energy reaction path of the proposed model surface based upon the available information. As it can be seen in this figure, the energy barriers increase when a collinear geometry ( $C_{\infty v}$ ) is imposed on both PESs. From these results it can be concluded that the approach of the  $N(^4S_u)$  atom to the  $NO(X^2\Pi)$  molecule will proceed through NNO angles not too far from that of the saddle point [ $108.9^\circ$  (Ref. 19)] at low and moderately low collision energies and will only begin to explore more repulsive configurations as collision energy is increased.

As has already been pointed out, Walch and Jaffe<sup>19</sup> performed CASSCF calculations followed by multireference contracted CI (hereafter referred to as CCI) on both triplet surfaces. In this work, the authors showed that the CASSCF barrier heights were consistently too high and that a substantial lowering was obtained within the CCI approach. Therefore, we have selected the CCI geometries and energies to carry out all subsequent calculations. As it can be seen in Table I, the barrier height for the  $^3A'$  PES lies well above the corresponding value for the ground  $^3A''$  surface. Therefore, the reactivity at relative energies below 0.6 eV will be well described using the  $^3A''$  surface only. As collision energy increases, the reaction channel corresponding to evolution on the  $^3A'$  surface will begin to pay

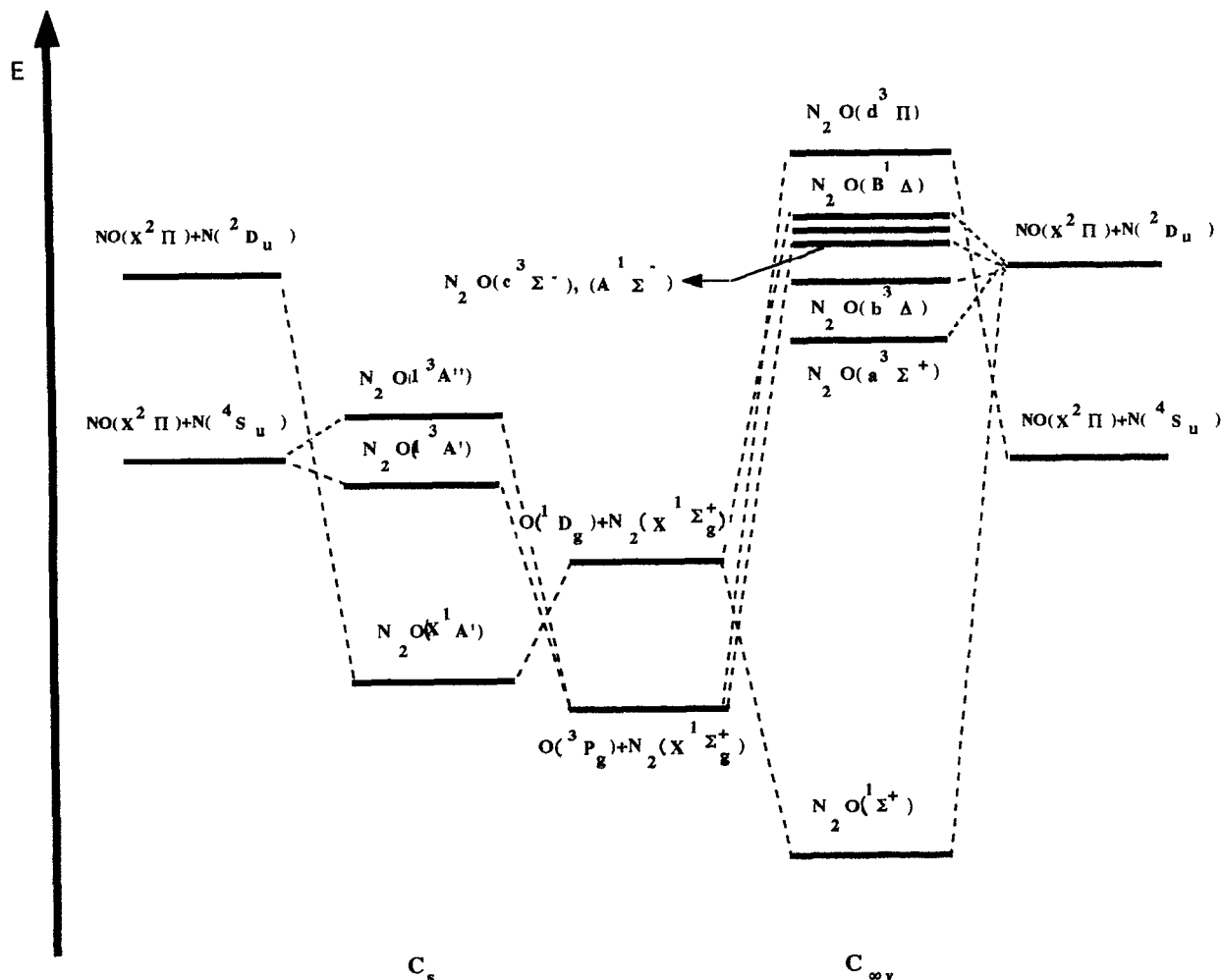


FIG. 1. Partial correlation diagram for  $N_2O$  molecules in  $C_s$  and  $C_{\infty v}$  symmetry. Data taken from Refs. 20–23.

a significant contribution to reactivity. In this study we have limited our calculations to the  $^3A''$  PES, but a dynamical study on the higher lying triplet ( $^3A'$ ) PES is in progress and will be reported in the near future.

### B. Construction of the potential energy surface

The analytical Sorbie–Murrell PES described elsewhere<sup>24–26</sup> has been used in the calculations. This function is based on the many-body expansion of the potential energy interaction, and for a triatomic system can be written as

$$V_{\text{NNO}}(R_1, R_2, R_3) = V_{\text{NN}}^{(2)}(R_1) + V_{\text{NO}}^{(2)}(R_2) + V_{\text{NO}}^{(2)}(R_3) + V_{\text{NNO}}^{(3)}(R_1, R_2, R_3). \quad (3)$$

The two body terms corresponding to the diatomics were fitted using extended Rydberg diatomic expressions.<sup>26</sup> Table II shows the coefficients of the extended Rydberg expansions used and the corresponding spectroscopic parameters derived from the fitting. The fitting is slightly worse for the  $NO(X^2\Pi)$  diatomic molecule for which we have chosen the  $NO(X^2\Pi_{1/2})$  spin orbit state parameters

for the fitting.<sup>21</sup> For the three-body term, the usual polynomial and range function expressions were employed.<sup>24–26</sup>

The *ab initio* information available about this system can be found elsewhere.<sup>19,27</sup> For the reasons discussed above, only the data referred to as contracted CI in Refs. 19 and 27 have been used for fitting purposes. Contrary to the strategy followed in similar studies,<sup>28,29</sup> where only the saddle point properties (energy, geometry, and harmonic force field) were used to construct an analytical Sorbie–Murrell PES, a procedure based on an overall fitting of the geometries and energies of the grid of *ab initio* points available has been designed.

Obtaining a suitable Sorbie–Murrell functional form for a given set of points involves finding the best set of polynomial coefficients of the three-body term that, for a fixed value of the hyperbolic tangent range function exponents, minimize the square of the differences between the calculated energy values and those computed with the Sorbie–Murrell analytical function at each geometrical configuration included in the grid. A linear least-squares algorithm<sup>30</sup> has been used for this purpose. This procedure has to be repeated for different sets of hyperbolic tangent

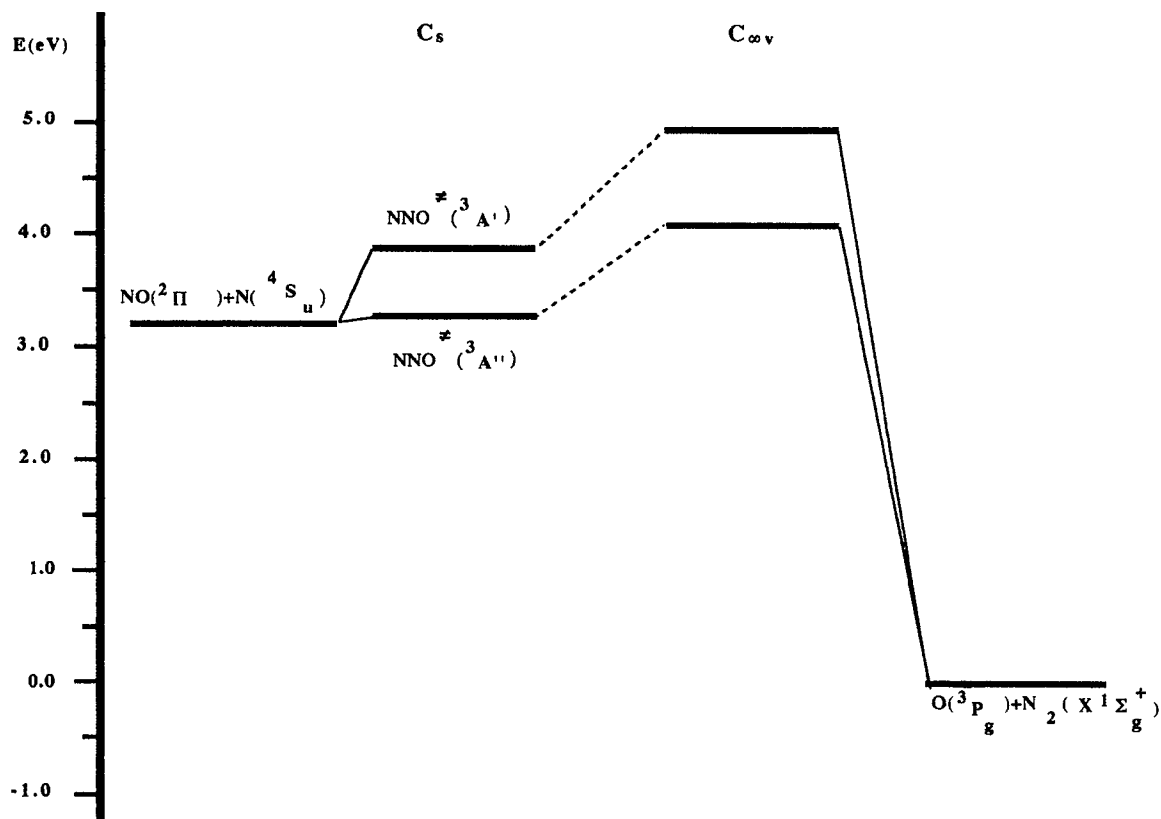


FIG. 2. Minimum energy reaction path diagram for the  $N+NO$  reaction in  $C_s$  and  $C_{\infty v}$  approaches. Data taken from Refs. 19–23.

exponents  $\gamma$  until the sum of the squares of the differences between the calculated and analytically derived energy values falls below a reasonable limit. This latter step involves usually tedious and time consuming work since there is not frequently a clear relationship between the changes in exponents and the overall behavior of the PES. In this work this last step has been sped up by replacing it with a non-linear least-squares procedure<sup>31</sup> in which the polynomial coefficients are held constant while the hyperbolic tangent exponents are left to vary. A reevaluation of the polynomial coefficients is then performed and the method goes on iteratively until convergence.<sup>32</sup> The usual procedure is to depart from a grid of integer exponents  $\gamma$ . For each point  $(\gamma_1, \gamma_2, \gamma_3)$  on the grid, the fitting program is asked to optimize both coefficients and exponents, even though it is possible to carry on optimizations for fixed values of the coefficients or exponents. Convergence is usually attained much faster for the exponents than for the polynomial co-

efficients so that 2 to 5 iterations are enough to achieve stability at each point.

At the start of the optimization process all points on the grid are usually assigned a weight of 1.0, so that the preliminary optimized Sorbie–Murrell surface provides an approach to the real shape of the final PES. Once the most suitable sets of parameters (coefficients and exponents) are obtained, it is necessary to tune up the surface so that the most important structural features such as the geometry and energies of the stationary points are very accurately reproduced. This tuning procedure requires a careful handling of the weights assigned to the points on the grid as well as a fine tuning of the range function exponents too. Once the accurate reproduction of the relevant structural features of the PES is achieved, the analytical surface obtained is checked for a possible spurious behavior in configurations for which no information is available.

It is to be noted that in this procedure no specific

TABLE I. Computed saddle point properties of both PESs for the  $N(^4S_u) + NO(X^2\Pi) \rightarrow N_2(X^1\Sigma_g^+) + O(^3P_g)$  reaction. Data taken from Ref. 19.<sup>a</sup>

PES	$\Delta E_b$	$R_{NN}$	$R_{NO}$	$\theta(NNO)$	$\nu_1$	$\nu_2$	$\nu_i$
$^3A''$	0.02	2.1707	1.1490	108.9	1785	315	210i
$^3A'$	0.62	1.8913	1.1695	116.5	1678	383	569i

<sup>a</sup>Energies in eV relative to reactants, distances in Å, angles in degrees, and frequencies in  $\text{cm}^{-1}$ .

TABLE II. Spectroscopic parameters and extended Rydberg parameters for the  $NO(X^2\Pi)$  and  $N_2(X^1\Sigma_g^+)$  diatomics.<sup>a</sup>

	$D_e$	$R_e$	$\nu_e$	$\nu_e x_e$	$a_1$	$a_2$	$a_3$
$NO(X^2\Pi)$	-6.6144	1.1508	1904.20	15.19	5.0352	5.1510	2.9980
$N_2(X^1\Sigma_g^+)$	-9.9051	1.0977	2358.57	14.32	5.3959	7.3281	4.9882

<sup>a</sup>Energies in eV relative to dissociated atoms, distances in Å, frequencies in  $\text{cm}^{-1}$ , and  $a_i$  coefficients in  $\text{Å}^{-1}$ ,  $\text{Å}^{-2}$ , and  $\text{Å}^{-3}$ , respectively.

TABLE III. Symmetry adapted coordinates ( $S_1, S_2, S_3$ ) and  $C_{2v}$  reference structure ( $R_1^0, R_2^0, R_3^0$ ) used in the fitting of the NNO ( $^3A''$ ) PES.<sup>a</sup>

$R_1^0 = 2.1707 \text{ \AA}$
$R_2^0 = R_3^0 = 1.9575 \text{ \AA}$
$S_1 = \rho_1$
$S_2 = (1/\sqrt{2})(\rho_2 + \rho_3)$
$S_3 = (1/\sqrt{2})(\rho_2 - \rho_3)$

<sup>a</sup> $R_i$ , as defined in Eq. (3) and  $\rho_i = R_i - R_i^0 \forall i$ .

constraint is imposed on the geometry and energy of the stationary points, since what is sought for is an overall reproduction of the shape of the PES. If this is achieved for configurations near the saddle point geometry, it is to be expected that this will cause the surface to show stationary points not far from the theoretical values.

The CCI grid used in the building of the  $^3A''$  surface consists of 20 points at an NNO angle of 110.0 deg, covering a variation in  $R_{NO}$  from 1.058 to 1.270 Å in 0.053 Å increments and a variation of  $R_{NN}$  from 1.850 to 2.380 Å in 0.264 Å increments, plus three points at 100.0 deg and three more points at 120.0 deg, for which  $R_{NO}$  is kept fixed at 1.642 Å and  $R_{NN}$  is varied from 1.850 to 2.380 Å in 0.264 Å increments. Besides, the NNO bending potential has also been included in the input, although other data from the *ab initio* grids of Ref. 27 describing the asymptotes were not incorporated to the fitting, since the two-body terms have already been set to reproduce the spectroscopic data of the asymptotes. The *ab initio* electronic energies had to be transformed to energies relative to the dissociated atoms limit. To get a smooth connection with the asymptotes made to fit the spectroscopic data, the electronic energy of the  $N + NO$  asymptote has been reevaluated by subtracting the electronic barrier height (0.5 kcal/mole) from the electronic energy of the saddle point and then assigned to the bottom of the  $NO(X^2\Pi)$  diatomic curve, placed  $-6.6144$  eV below the dissociation plateau. The energy of the points of the grid with respect to dissociated atoms was then obtained by subtracting the electronic energy of reactants from their energies.

An important feature of the Sorbie–Murrell expansion is the possibility of using symmetry adapted coordinates for systems in which symmetry restrictions must hold. In the case of the  $N + NO$  system, the PES must remain invariant with respect to exchange of both nitrogen atoms. Table III shows the symmetry adapted coordinates ( $S_1, S_2, S_3$ ) and reference structure ( $R_1^0, R_2^0, R_3^0$ ) used in this case. To keep the PES invariant with respect to N atom exchange, the coefficient of any polynomial or exponential term containing the antisymmetric coordinate with odd powers must be zero.<sup>26</sup> The number of parameters left for optimization is then somewhat reduced.

The first attempts at obtaining a reasonable PES led to a good fitting of the grid of *ab initio* points but produced surfaces with deep minima near the corner of the PES, corresponding in fact to the short distance range. These deep wells are caused by the combination of the attractive contributions of the diatomic potentials for NO and NN in the zone where both  $R_{NN}$  and  $R_{NO}$  distances are near the

equilibrium geometry (cf. Fig. 3). The saddle point geometry corresponds to an early energy barrier placed into the reactant valley and no points in the *ab initio* grid cover the zone where the two-body contributions [ $V_{NN}^{(2)}(R_1) + V_{NO}^{(2)}(R_2) + V_{NO}^{(2)}(R_3)$ ] are more important. Thus the fitting procedure is unable to generate a three-body term repulsive enough to compensate for the attractive contribution of the two-body terms in this zone.

The obvious solution to this problem consisted in calculating *ab initio* points in the short distance range. Thus an additional grid of points for  $R_{NN}$  varying between 1.1 and 2.1 Å and  $R_{NO}$  moving from 1.1 to 1.5 Å was evaluated using the CASSCF method with a split valence basis set including polarization. The quality of this CASSCF calculation was similar to that reported in Ref. 19. Even though the results for the saddle point geometry and bending potential were rather encouraging it was not possible to achieve a smooth connection between these data and the better CCI points already available, thus giving rise to instabilities in the fitting.

Having ruled out additional *ab initio* calculations, a more cautious approach based upon empirical corrections to the grid was adopted. First, an initial grid of 100 hyperbolic tangent exponents ( $\gamma_1, \gamma_2$ ) with  $\gamma_1$  and  $\gamma_2$  ranging between 0.0 and 9.0 Å<sup>-1</sup> ( $\gamma_3$  is constrained to be 0 on symmetry considerations<sup>26</sup>) was used for optimization considering a Sorbie–Murrell polynomial up to the third degree. From the final sets of  $\gamma$  obtained, only those showing the lowest discrepancies (one standard deviation) in energy from the original grid of *ab initio* points were selected. Contour plots for these optimal initially selected sets of coefficients were then produced and those not leading to realistic PES were discarded. This is a rather cumbersome step, since many sets of exponents usually lead to energetically reasonable fittings, given the small number of points on the grid, not corresponding however to physically meaningful PESs.

With those PESs exhibiting a reasonable behavior, we carried out a study of the contribution of the values of the exponents  $\gamma$  to the shape of the PES. It was not however possible to suppress a spurious minimum at the corner of the PES for any of the exponent combinations considered. A minimization program<sup>33</sup> was then used to study the evolution of this spurious minimum, obtaining the geometrical configurations of minimal energy at fixed values of the NNO angle starting from  $R_{NO}$  and  $R_{NN}$  bond distance values around those of the minima on the corner of the PES. After this, we generated a set of interpolated points around the minimum at each fixed angular value. For these sets of points, energy was made to vary smoothly from reactives to products, leveling off the zone around the minima. Since the number of *ab initio* points available is rather scarce, it was enough to introduce a set of interpolated points for just one angular value to induce substantial changes in the shape of the PES. We found out that the interpolation was most effective for an NNO angle of 100 deg. In order to downplay any effect caused by the connection of the empirical and *ab initio* data, the weight of the points of the interpolated set was lowered to 0.7. After

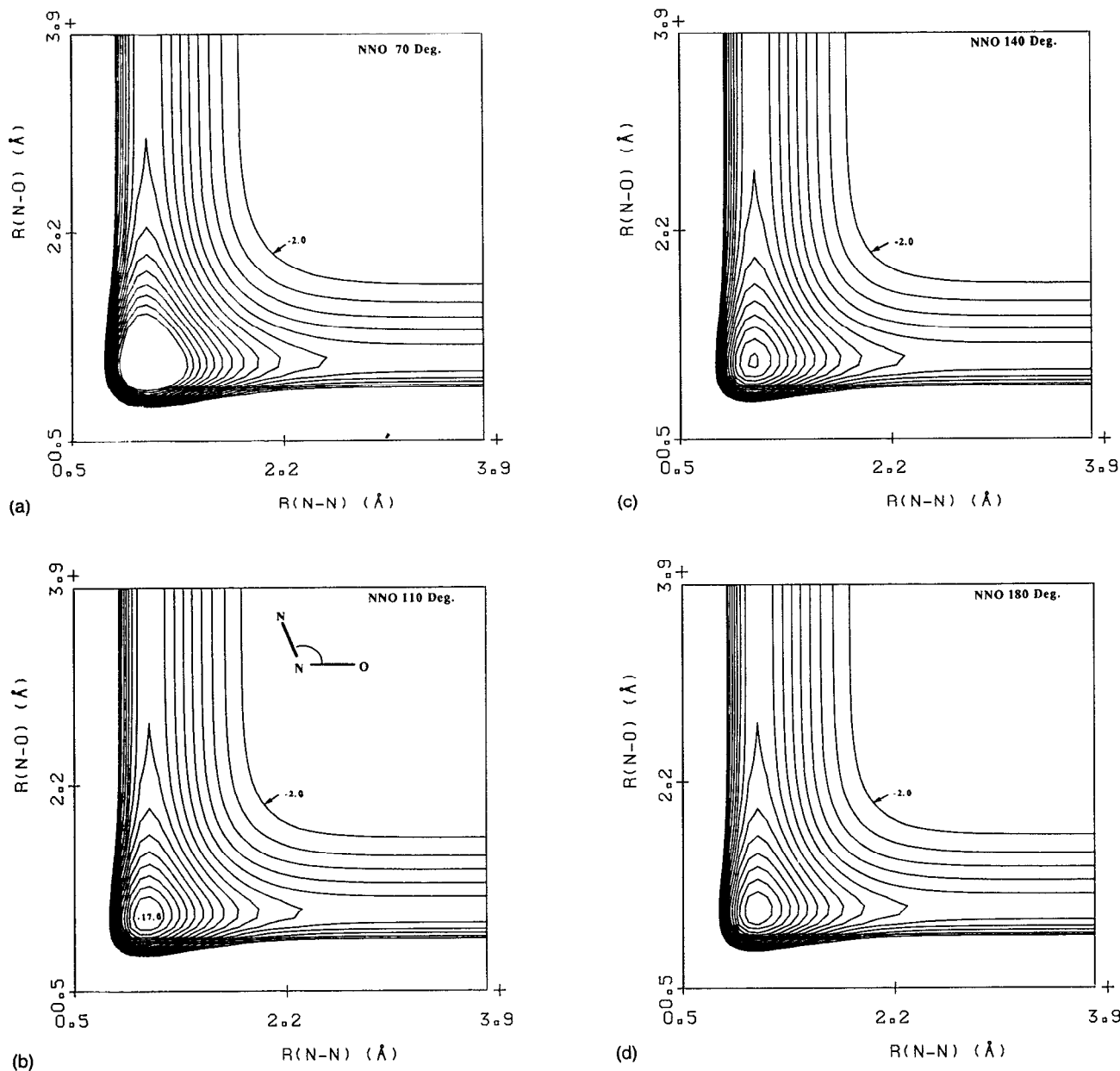


FIG. 3. Equipotential contours of the two-body potential of the  $NNO(^3A'')$  system. Contours are spaced by 1.0 eV with energies relative to dissociated atoms.

this, the  $\gamma_1$  and  $\gamma_2$  exponents were let optimize until convergence, and their final values were  $\gamma_1=1.315 \text{ \AA}^{-1}$  and  $\gamma_2=2.327 \text{ \AA}^{-1}$ . In Table IV the optimal three-body parameters of the analytical Sorbie–Murrell function are shown. This surface reproduced the *ab initio* points with a mean square deviation in energy of  $\sigma^2=0.002 \text{ eV}^2$  and a standard deviation  $\sigma=0.046 \text{ eV}$  (1.06 kcal/mol).

### C. Analysis of the optimal surface

Figure 4 shows equipotential contour plots of the final optimal PES. As it can be seen in the figure, the surface evolves smoothly from a repulsive configuration at NNO angles around  $180^\circ$  to a situation with no apparent barrier at  $110^\circ$ . If the angle is narrowed further to  $70^\circ$ , the  $-6.0 \text{ eV}$

TABLE IV. Three-body parameters of the analytical  $^3A''$  PES.<sup>a</sup>

$V_0$	0.954	$c_{111}$	2.360	$\gamma_1$	1.315
$c_1$	0.535	$c_{112}$	-4.756	$\gamma_2$	2.327
$c_2$	-3.455	$c_{113}$	0.000	$\gamma_3$	0.000
$c_3$	0.000	$c_{122}$	-3.054		
$c_{11}$	4.951	$c_{123}$	0.000		
$c_{12}$	-5.724	$c_{133}$	-2.024		
$c_{13}$	0.000	$c_{222}$	1.497		
$c_{22}$	-0.254	$c_{223}$	0.000		
$c_{23}$	0.000	$c_{233}$	3.589		
$c_{33}$	-0.191	$c_{333}$	0.000		

<sup>a</sup> $V_0$  in eV,  $c_i$  in  $\text{\AA}^{-1}$ ,  $c_{ij}$  in  $\text{\AA}^{-2}$ ,  $c_{ijk}$  in  $\text{\AA}^{-3}$ , and  $\gamma_i$  in  $\text{\AA}^{-1}$ .

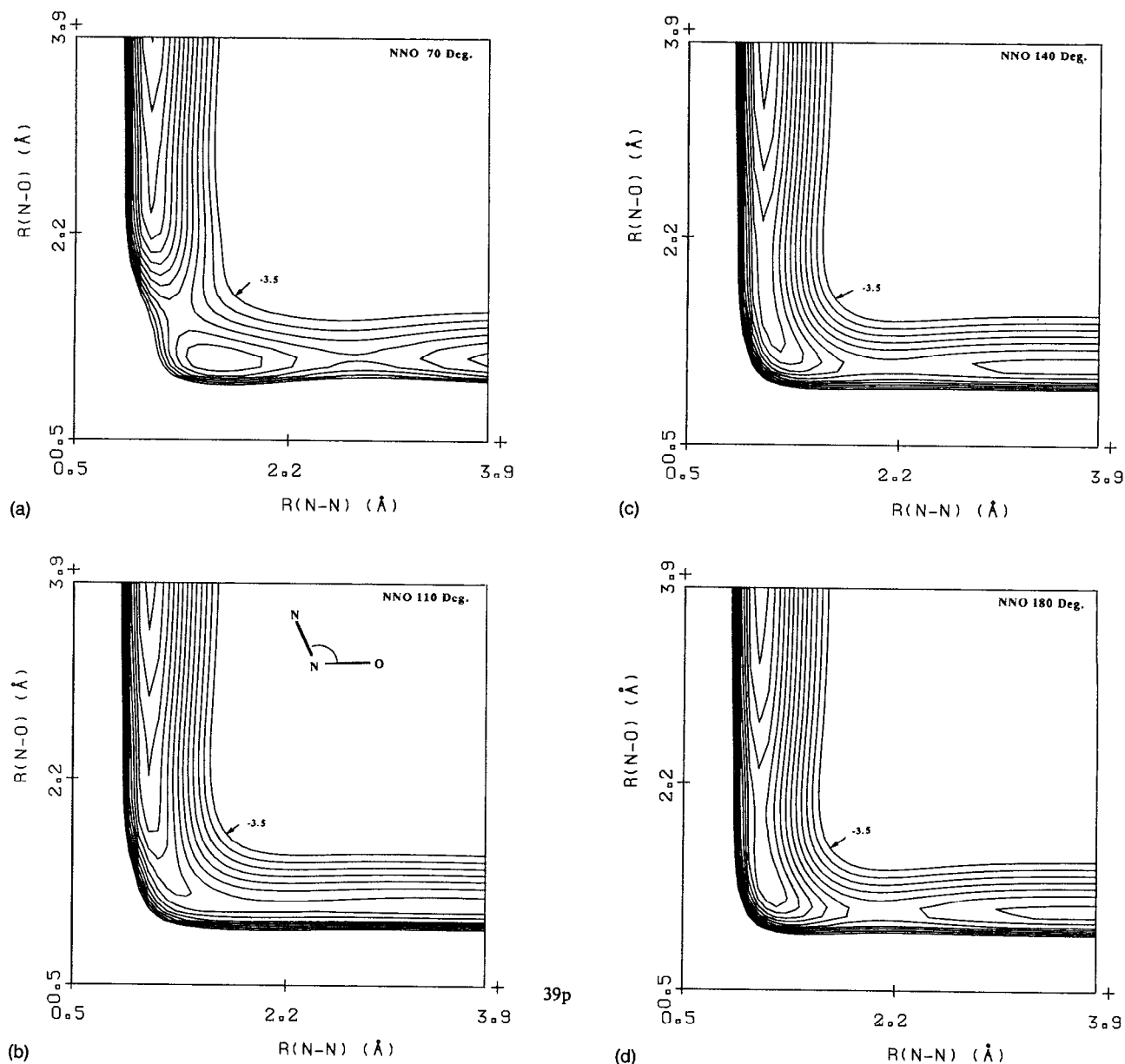


FIG. 4. Equipotential contours of the two plus three-body optimal potential of the  $NNO(^3A'')$  system. Contours are spaced 0.5 eV with energies relative to dissociated atoms.

equipotential curve breaks into a well in the entrance channel placed  $-0.4$  eV below reactants and separated from products by a barrier of 0.4 eV relative to the bottom of the well. Closing the angle even more causes the barrier height to rise to more than 2 eV. Figure 5 shows a plot of the theoretical and fitted NNO bending potential at the  $R_{NN}$  and  $R_{NO}$  saddle point values. The agreement between both sets of values is excellent.

To locate possible spurious accidents on the fitted PES as well as to characterize exactly the saddle point geometry on this surface, a reaction coordinate considering the N approach to NO following the minimum energy reaction path has been carried out. As the N atom approaches the NO molecule, the energy decreases from the asymptotic value of  $-6.6144$  eV to a minimal value of  $-6.7529$  eV

(0.1358 eV below reactants) at a  $R_{NN}$  distance of  $3.4$  Å. A force constant analysis of this point evidenced that it corresponded indeed to a very shallow minimum. Such spurious long-range minima are often found for Sorbie-Murrell fittings. This is a handicap of this kind of fitting,<sup>34</sup> although it is to be expected that its influence on the dynamics of the reaction will be negligible. After this first minimum, the energy rises until it reaches a maximal value of  $-6.6161$  eV for  $R_{NN}=2.2800$  Å,  $R_{NO}=1.1461$  Å,  $\theta_{NNO}=107.10^\circ$ . This point would correspond to the  $NNO^3A''$  saddle point. The agreement with the *ab initio* saddle point geometry and energy values given in Ref. 19 ( $R_{NN}=2.1706$  Å,  $R_{NO}=1.1494$  Å,  $\theta_{NNO}=108.9^\circ$ ,  $E=-6.5927$  eV) is quite good, the largest discrepancy (5.04%) being obtained for the  $R_{NN}$  distance. In principle, the most serious drawback for

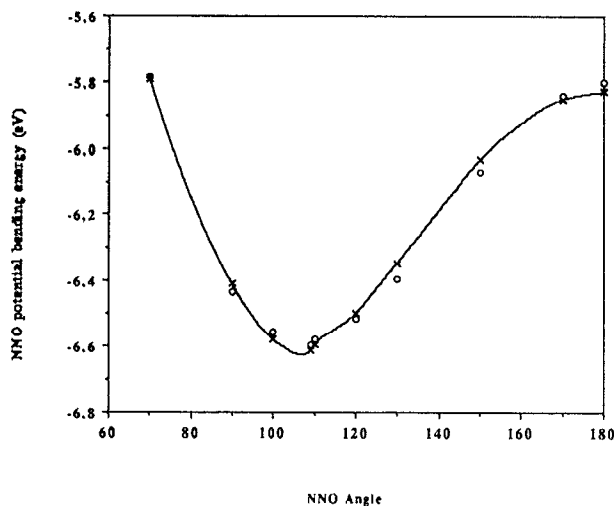


FIG. 5. *Ab initio* CCI (Ref. 19) (o) and fitted ( $\times$ ) bending potentials on the analytical PES with  $R_{NO}$  and  $R_{NN}$  fixed at the *ab initio* saddle point values. Energies in eV relative to dissociated atoms.

the saddle point estimate is that it falls almost 0.54 kcal/mol below the value derived from the *ab initio* calculations (0.0017 eV below the reactants asymptote). Nonetheless, this does not in fact affect the validity of this surface for dynamical calculations. As a matter of fact, as was already remarked by Walch and Jaffe,<sup>19</sup> reaction (1) proceeds most likely with no barrier, and a further improvement of their *ab initio* calculations would most surely result in the energy barrier vanishing. The frequencies for the saddle point of the fitted PES (119i, 421, and 1858  $\text{cm}^{-1}$ ) are also in quite good agreement with those reported in Ref. 19 (210i, 381, and 1785  $\text{cm}^{-1}$ ) with the exception of the imaginary frequency.

From the entrance saddle point following the minimum energy path, the energy falls until it reaches a very shallow spurious minimum on the corner of the PES placed 1.44 eV above products. These are in fact the remainings of the spurious minima referred to above, albeit reduced to a much more limited angular scope and energy depth. This spurious accident, being placed well down on the path leading to products, will probably have a negligible influence on the dynamics of the system. Following the minimum energy path, we come to the exit saddle point for the passage to products, placed 0.16 eV above the bottom of the minimum. Further tunings of the surface to eliminate these accidents would require a great amount of time without leading, probably, to a significant improvement in the reaction dynamics and have therefore been left out.

Unfortunately, it has not been able to compare the present fitted PES with the existing modified LEPS one of Jaffe *et al.*,<sup>18</sup> since no information about the parameters used for the building of this latter one is available, nor is there to the best of our knowledge, any published description of the main features of the analytical function used in Ref. 18.

TABLE V. Dynamical properties for  $N + NO$  ( $v=0, J=7$ )  $\rightarrow N_2 + O$  reaction as a function of  $E_T$ .<sup>a</sup>

$E_T$	$S_r$	$\langle f_T' \rangle^b (\delta E_T)^c$	$\langle f_v' \rangle^b (\delta E_{vib})^c$	$\langle f_r' \rangle^b (\delta E_{rot})^c$	$f/b^d$
0.0388	$1.06 \pm 0.09$	0.63(2.15)	0.28(0.87)	0.08(0.27)	0.03
0.1	$2.82 \pm 0.09$	0.64(2.14)	0.27(0.84)	0.09(0.31)	0.14
0.2	$4.43 \pm 0.26$	0.64(2.12)	0.26(0.84)	0.10(0.34)	0.26
0.3	$5.52 \pm 0.10$	0.64(2.07)	0.26(0.83)	0.11(0.39)	0.35
0.5	$6.51 \pm 0.22$	0.67(2.13)	0.20(0.67)	0.13(0.49)	0.50
0.6	$7.00 \pm 0.10$	0.66(2.07)	0.21(0.71)	0.13(0.51)	0.57
0.8	$7.31 \pm 0.13$	0.65(1.92)	0.21(0.78)	0.14(0.59)	0.62
1.0	$7.12 \pm 0.16$	0.62(1.75)	0.22(0.87)	0.15(0.67)	0.77
1.5	$7.25 \pm 0.11$	0.60(1.45)	0.24(1.06)	0.16(0.78)	1.17
1.8	$7.29 \pm 0.11$	0.58(1.24)	0.26(1.22)	0.16(0.83)	1.26

<sup>a</sup> $S_r$  in  $\text{\AA}^2$ , and  $E_T$ ,  $\delta E_T$ ,  $\delta E_{vib}$ , and  $\delta E_{rot}$  in eV.

<sup>b</sup>Average fraction of available energy appearing as translation ( $\langle f_T' \rangle$ ), vibration ( $\langle f_v' \rangle$ ), and rotation ( $\langle f_r' \rangle$ ) in products.

<sup>c</sup>Increments in translational, vibrational, and rotational energies when evolving from reactants  $N + NO$  to products  $N_2 + O$  (see text).

<sup>d</sup>Ratio of forward vs backward scattered reactive trajectories in the center of mass framework.

### III. QUASICLASSICAL TRAJECTORY CALCULATIONS

#### A. Computational method

Preliminary quasiclassical trajectory calculations (QCT) for reaction (1) on the Sorbie–Murrell PES described above have been performed using a QCT program developed in our laboratory.<sup>35</sup> The integration methods and Monte Carlo samplings are identical to those employed in previous studies.<sup>36–38</sup> Since the aim was to test the validity of the surface against the available experimental kinetic and dynamical data, trajectories were run only for the most populated rovibrational level of NO at 300 K,  $v=0, J=7$  within the nonrigid rotor and anharmonic oscillator approximation. For this rovibrational state, a range of collisional energies ( $E_T$ ) relative to the center of mass of the system from 0.0388 to 1.8 eV was considered. For each  $E_T$  value, enough trajectories were calculated to guarantee that statistical errors (one standard deviation) in total cross section fall below 10%. In spite of the low relative energy values explored, an analysis of the convergence of the numerical integration of the equations of motion using back integration showed that the number of poorly converged trajectories was negligible when compared with the amount of reactive ones. In all, about 52 000 trajectories were computed on the IBM 3090/600J computer of the Centre de Supercomputació de Catalunya.

#### B. Excitation function and thermal rate constant

As it has already been pointed out, since the PES used for reaction (1) shows no barrier for the passage to products, reactive trajectories have been observed over the whole energy range studied.

For the  $v=0, J=7$  level of NO, Table V shows the  $E_T$  dependences of the total reactive cross section ( $S_r$ ), the average translational ( $\overline{E}_T'$ ), vibrational ( $\overline{E}_{vib}'$ ), and rotational ( $\overline{E}_{rot}'$ ) energy values of products given as fractions of the available energy and also, in parentheses, expressed as  $\overline{E}_i' = E_i + \delta E_i$ ,<sup>37</sup> and the forward/backward ratio of reactive



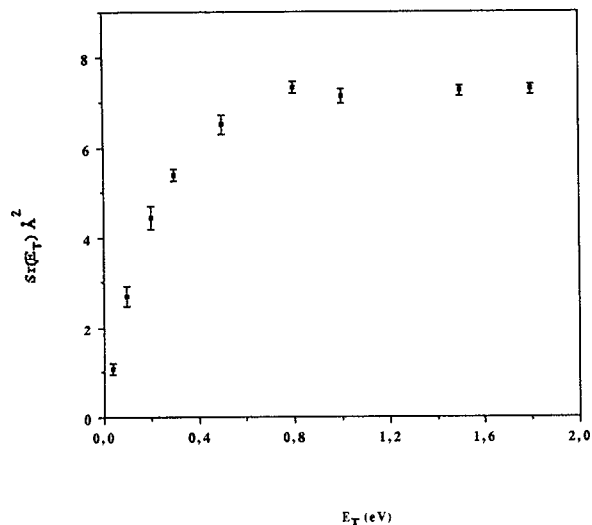


FIG. 6. Excitation function for the  $N + NO(v=0, J=7) \rightarrow N_2 + O$  reaction.

trajectories scattered in the center of mass framework. The excitation function plot is depicted in Fig. 6.  $S_r$  rises with  $E_T$  until it reaches a shallow plateau above 0.8 eV, this behavior conforms to that of a reaction exhibiting an energy threshold.<sup>39</sup>

The rise in the absolute cross section as energy is increased can be explained in terms of the shape of the PES. As it becomes evident from Fig. 5, the bending potential at the saddle point bond distances rises steeply as the NNO angle is moved away from the saddle point *ab initio* CCI value [108.9° (Ref. 19)], even though the rise is steeper for narrower angles. While trajectories reaching configurations close to the saddle point with energy above the corresponding NNO bending energy value could lead to reaction, at low energies only those trajectories reaching configurations with NNO angles close enough to that of the saddle point will eventually lead to products. As  $E_T$  is increased, the scope of angular configurations leading to reaction is enlarged. On the other hand, since the rise in bending energy is steeper for smaller NNO angles, the reaction window will expand less in this direction. The overall effect is an augmentation of  $S_r$  with  $E_T$ . Up from a certain relative energy value, all angles from that of the saddle point to 180° contribute to reactivity, but since the reaction window enlarges very little in the narrow angle zone  $S_r$  tends to saturation,<sup>40</sup> showing a plateau, as observed in Fig. 6.

Since no experimental data on  $S_r$  are available from the literature, we have estimated the thermal rate constant at 300, 500, and 700 K using the excitation function for reaction (1) with the NO molecule placed at the most populated rovibrational level ( $v=0, J=7$ ) at 300 K. The excitation function values were fitted to a fifth degree polynomial in relative energy and the resulting expression was integrated using the standard equation<sup>39</sup> to obtain the state specific rate constant. Even though this value cannot be compared directly with the experimental measurements, it may provide a good assessment of the ability of the PES

TABLE VI. Experimental rate constant and trajectory estimate at several temperatures.<sup>a</sup>

300		T(K)		700		Reference
		500				
$> 4.0 \times 10^{11}$						4
$(1.3 \pm 0.4) \times 10^{13}$						5
$(1.5 \pm 0.8) \times 10^{13}$ <sup>b</sup>		$(2.3 \pm 0.9) \times 10^{13}$ <sup>b</sup>		$(2.9 \pm 1.0) \times 10^{13}$ <sup>b</sup>		6
$(2.0 \pm 0.5) \times 10^{13}$						7
		2.1 to $2.3 \times 10^{13}$ in the 476-755 K interval				9
$(1.0 \pm 0.5) \times 10^{13}$						10
$(1.8 \pm 0.6) \times 10^{13}$						12
$(1.6 \pm 0.3) \times 10^{13}$						13
$(1.5 \pm 0.1) \times 10^{13}$		$(3.0 \pm 0.3) \times 10^{13}$		$(4.9 \pm 0.3) \times 10^{13}$		This work

<sup>a</sup>Rate constant in  $\text{cm}^3/\text{mol s}$ .

<sup>b</sup>Determined from the  $k$  vs  $T$  dependence given in Ref. 6.

to reproduce the kinetic features observed. Table VI evidences a good agreement between the trajectory estimate and the experimental results at the different temperatures considered.

The accord is particularly good at 300 K, where the value derived from the present preliminary calculations falls within the error interval of Refs. 5–7 and 12. Our estimate practically reproduces the recommended value reported by Baulch *et al.*<sup>13</sup> at 300 K. At higher temperatures the agreement between our trajectory values and the experimental results is not so good. These discrepancies may arise from the fact that only the most populated rovibrational level of NO at 300 K has been considered in the QCT calculations. The NO mass combination causes the rovibrational population of NO molecules to be in fact scattered over a considerable number of levels. Once calculations have been performed for a number of rovibrational levels covering a significant percentage of the NO population at these temperatures,<sup>40</sup> the calculated  $k$  value may come even closer to the experimental results.

While direct comparison between the present results and those of Jaffe *et al.* for the inverse reaction is not possible, it seems that the enhancement of reactivity with  $E_T$  found in the present study is consequent with the observed trend toward favoring reactivity as the vibrational energy of reactants is increased reported in Ref. 18 for the inverse reaction.

### C. Energy disposal in products

For all values of the relative energy considered, the average fractions of available energy going into translation  $\langle f'_T \rangle$ , vibration  $\langle f'_v \rangle$ , and rotation  $\langle f'_r \rangle$  of products are comprised in the 0.6–0.7, 0.2–0.3, and 0.1–0.2 intervals, respectively (Table V). For  $E_T$  between 0.038 88 and 1.0 eV the increments in translational ( $\delta E_T$ ), vibrational ( $\delta E_{\text{vib}}$ ), and rotational ( $\delta E_{\text{rot}}$ ) energies range between 1.8–2.2, 0.7–0.9, and 0.3–0.7 eV, respectively (Table V). As for the  $E_T$  dependence,  $\langle f'_T \rangle$  and  $\delta E_T$  are essentially constant (with the only exception of what occurs for the  $\delta E_T$  values at the higher relative energies explored),  $\langle f'_v \rangle$  and  $\delta E_{\text{vib}}$  exhibit a minimum at around 0.5 eV, and  $\langle f'_r \rangle$  and  $\delta E_{\text{rot}}$  increase monotonously with  $E_T$ . Since the reduced masses

of reactives and products are very similar, these facts do not probably come from kinematic constraints and should be attributed instead mainly to the effects of the shape of the PES.<sup>40</sup> Assuming that more open NNO angles than that of the saddle point will cause similar distributions of available energy in products, as  $E_T$  increases the system will be able to explore more bent configurations along the path leading to products. The overall effect will thus be an increase in  $E'_{rot}$  and  $\langle f'_r \rangle$  as relative energy is increased.<sup>41,42</sup>

Another interesting feature depicted in Table V is the forward/backward ( $f/b$ ) scattering ratio increase with rising  $E_T$ . At the lowest collision energy, practically all reactive trajectories are scattered backward in the center of mass framework. This would point toward energy being released mainly as repulsion in the direction of the NO bond immediately after both NN atoms have reached a distance not far from that of the  $N_2$  bond distance. As the N atom approaches the NO molecule, the steep downhill variation of the potential leading from the saddle point to products tends to accelerate the trajectory thus causing a sudden approach of the N atom to the NO molecule, as has been confirmed by inspection of individual reactive trajectories. The very repulsive nature of the NNO adduct formed would result in energy being released along the direction of the NO bond. As  $E_T$  increases enough, the inertial effect probably becomes dominant and the NO molecule formed is produced mainly in the direction of the attacking N atom.

Experimental Refs. 14 and 17, give  $0.28 \pm 0.07$  and  $0.25 \pm 0.03$  for the fraction of exothermicity released as vibration, which correspond to mean vibrational energy contents of products of  $0.87 \pm 0.22$  and  $0.82 \pm 0.09$  eV, respectively (or  $0.25 \pm 0.06$  and  $0.24 \pm 0.03$  of the available energy, respectively). The QCT value at thermal relative energy ( $E_T = 0.0388$  eV) is  $0.97 \pm 0.4$  eV ( $0.28 \pm 0.11$  in fraction of available energy), in very good accord with experimental results. The important errors in the fractions of energy going into the different modes of products at the lowest relative energy studied ( $0.64 \pm 0.14$ ,  $0.28 \pm 0.11$ , and  $0.08 \pm 0.06$  for translation, vibration, and rotation, respectively) are caused by the modest statistics (low proportion of reactive trajectories) so far reached at this energy.

#### D. Vibrational distribution of products

Figure 7 shows the vibrational distribution of the  $N_2$  molecules produced from reaction (1) with  $NO(X^2\Pi)$  molecules in the  $v=0, J=7$  rovibrational state at different  $E_T$  values.

As it can be seen in Fig. 7(a), an  $N_2$  vibrational inversion occurs for  $v'=2$  at 0.0388 and 0.3 eV. Even though for the lowest relative collision energy explored (0.0388 eV) the statistical errors (one standard deviation) are large, the vibrational inversion continues to appear at higher relative energy values where statistical uncertainties are much smaller. As  $E_T$  increases this inversion gradually diminishes, vanishes at  $E_T \geq 0.5$  eV, and comes closer to the statistical limit [Fig. 7(b)].<sup>43</sup> This kind of behavior, though not very usual, has also been found for other systems such

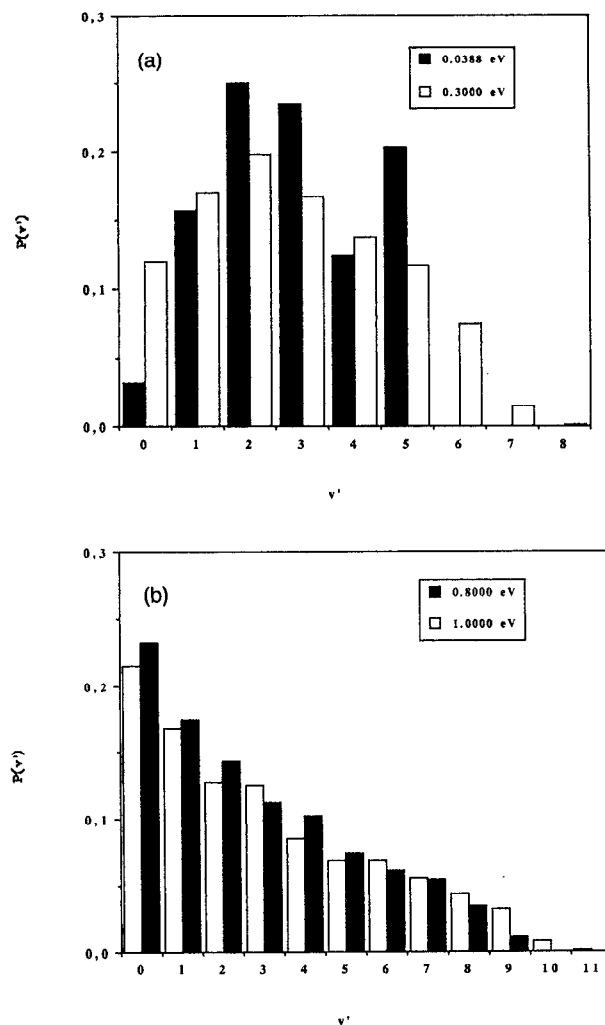


FIG. 7. Vibrational population distribution of  $N_2$  formed in the  $N + NO(v=0, J=7)$  reaction at different relative collision energies (eV): (a) 0.0388 (black) and 0.3 (white); (b) 0.8 (black) and 1.0 (white).

as  $H + HI$ ,<sup>38</sup> for which the vibrational inversion does also disappear with growing  $E_T$ . It is usually considered that an increase in the relative translational energy of reactants diminishes the time left for energy randomization, thus implying less statistical vibrational distributions as  $E_T$  is raised. However, it must also be taken into account that as relative collision energy increases, the main features of the potential become less relevant for the dynamics and the system can proceed through a wider range of configurations on its way to reaction. Hence, for those systems, such as the one considered in the present study, for which the shape of the PES exhibits a rather repulsive behavior when moving away from the saddle point configuration playing thus a major role in determining the reaction mode and consequently also the way energy is distributed among the different modes in products, the orientation effect may become dominant and lead to distributions resembling more the statistically expected ones when  $E_T$  is increased, especially also if the interaction time does not vary very much with  $E_T$ . In the case of the  $N + NO$  system, a preliminary analysis of the trajectories at different energies, indicates

that they proceed in a direct mode over the whole energy range, implying that the interaction time for energy randomization does not probably vary much for all  $E_T$  conditions considered. To check the influence of the NNO orientation angle on the vibrational distribution in products, we have performed an analysis of the NNO angle near the saddle point configuration for the reactive trajectories, monitoring also the vibrational population of  $N_2$  molecules formed in levels  $v'=0, 1$ , and  $2$ . For trajectories evolving with NNO angles near that of the saddle point ( $107.10^\circ$ ), a vibrational inversion situation with  $v'=1$  and  $v'=2$  more populated than  $v'=0$  and  $v'=1$ , respectively, is found. Instead, in those trajectories exploring NNO angles more open than that of the saddle point, a trend toward populating levels above  $v'=2$  is observed, probably because in these cases the incoming N atom tends more to compress the NO bond, giving rise to a greater  $N_2$  vibrational excitation. Conversely, for NNO configurations more bent than that of the saddle point, the vibrational inversion situation disappears and the  $v'=0$  level becomes the most populated one, with most of the  $N_2$  product vibrational population appearing in levels between  $v'=0$  and  $v'=2$ . For  $E_T=0.0388, 0.1, 0.3$ , and  $0.6$  eV, the scopes of NNO angular configurations near the saddle point leading to reaction are, respectively,  $100^\circ\text{--}125^\circ$ ,  $95^\circ\text{--}135^\circ$ ,  $85^\circ\text{--}145^\circ$ , and  $80^\circ\text{--}165^\circ$ , evidencing the opening of the reaction window as  $E_T$  is increased. Hence, at low energies most trajectories evolve through NNO configurations leading to vibrational inversion, while on growing  $E_T$  an ever more significant number of trajectories proceed through NNO bent configurations, which populate preferentially the  $v'=0$  level, and also through NNO configurations closer to collinear which favour  $v' > 2$  levels. Thus it can be seen that the constraints which limit the vibrational distribution in products vanish progressively with increasing relative energy, causing the  $v'=2$  vibrational inversion situation to disappear gradually.

Although vibrational inversion has been found experimentally,<sup>14,15</sup> the estimate of a percentage of  $75\% \pm 5\%$  of  $N_2$  molecules from reaction (1) formed with  $v' > 4$  obtained from ozone decomposition at thermal energies<sup>14</sup> does not in fact compare well with our calculations (35% of molecules produced with  $v' > 4$ ). No mention is made in Ref. 14 of translationally hot  $N_2$  molecules. However, according to our trajectory results, a significant fraction of the available energy should be released as translation of  $N_2$ . Even though vibration–translation energy transfer is usually slower than vibration–vibration relaxation,<sup>43</sup> the possibility that part of the ozone in Ref. 14 may have reacted through collisions with translationally hot  $N_2$  molecules might perhaps be invoked as a tentative explanation for the discrepancies between our theoretical and the experimental results.

#### IV. CONCLUSIONS

A Sorbie–Murrell functional form for the lowest  $^3A''$  PES of the  $N(^4S_u) + NO(X^2\Pi)$  system has been derived from a grid of *ab initio* points around the saddle point configuration. It has been shown that the lack of *ab initio*

data in the zone where the interatomic distances are close to the equilibrium bond distances of the diatomic molecules leads to deep minima on the surface. To suppress those minima, a fitting procedure based upon successive refinements of the PES with the introduction of a small grid of empirically interpolated points has been devised. The final PES obtained reproduced very well the *ab initio* information available, even though the calculated saddle point energy falls a little below the *ab initio* value.

Preliminary QCT calculations have been carried out on this surface for the most populated rovibrational level of NO at 300 K. The rate constants estimated from these calculations, as well as the fraction of available energy going into vibrational energy in products agree very well with the experimental data available. Vibrational inversion of products is found for the lowest energies explored, even though this distribution seems to be cooler than an experimental estimate. The vibrational inversion is lost when relative energy is increased, leading for the highest relative energy values to a distribution resembling more the statistical one. The very repulsive behavior of the PES as the angle is varied away from the saddle point value, as well as the high-energy difference between reactants and products should play a paramount role in determining the shape of the excitation function, the fraction of energy going into the different modes of products and the vibrational distribution of the  $N_2$  molecules formed.

#### ACKNOWLEDGMENTS

This work has been partially supported by the Dirección General de Investigación Científica y Técnica of the Spanish Ministry of Science and Education (DGICYT, Project PB88-0189). We would also like to thank the Centre d'Informàtica de la Universitat de Barcelona and the Centre de Supercomputació de Catalunya (CESCA) for computer time and facilities made available for this work.

- <sup>1</sup>M. Kh. Karapet'yants and M. L. Karapet'yants, *Thermodynamic Constants of Inorganic and Organic Compounds* (Ann Arbor-Humphrey, Ann Arbor, 1970).
- <sup>2</sup>D. F. Strobel, *J. Geophys. Res.* **76**, 8384 (1971).
- <sup>3</sup>G. Brassens and M. Nicolet, *Planet. Space Sci.* **21**, 939 (1973).
- <sup>4</sup>G. B. Kistiakowsky and G. G. Volpi, *J. Chem. Phys.* **27**, 1141 (1957).
- <sup>5</sup>L. F. Phillips and H. I. Schiff, *J. Chem. Phys.* **36**, 1509 (1962).
- <sup>6</sup>M. A. A. Clyne and I. S. McDermid, *J. Chem. Soc. Faraday Trans.* **71**, 2189 (1975).
- <sup>7</sup>J. H. Lee, J. V. Michael, W. A. Payne, and L. J. Stief, *J. Chem. Phys.* **69**, 3069 (1978).
- <sup>8</sup>M. Koshi, M. Yoshimura, K. Fukuda, H. Matsui, K. Saito, M. Watanabe, A. Imamura, and C. Chen, *J. Chem. Phys.* **93**, 8703 (1990).
- <sup>9</sup>M. A. A. Clyne and B. A. Thrush, *Proc. R. Soc. London Ser. A* **261**, 259 (1961).
- <sup>10</sup>J. T. Herron, *J. Chem. Phys.* **61**, 35 (1978).
- <sup>11</sup>Y. Takezaki and S. Mori, *Bull. Inst. Chem. Res. Kyoto* **45**, 388 (1967).
- <sup>12</sup>C. L. Lin, D. A. Parker, and F. Kaufman, *J. Chem. Phys.* **53**, 3896 (1970).
- <sup>13</sup>D. L. Baulch, D. D. Drysdale, and D. G. Haine, *Evaluated Kinetic Data for High Temperature Reactions* (Butterworths, London, 1973), Vol. 2.
- <sup>14</sup>J. E. Morgan, L. F. Phillips, and H. I. Schiff, *Discuss. Faraday Soc.* **33**, 118 (1962).
- <sup>15</sup>J. E. Morgan and H. I. Schiff, *Can. J. Chem.* **41**, 903 (1963).

- <sup>16</sup>K. L. Wray, E. V. Feldman, and P. F. Lewis, *J. Chem. Phys.* **53**, 4131 (1970).
- <sup>17</sup>G. Black, R. L. Sharpless, and T. G. Slanger, *J. Chem. Phys.* **58**, 4792 (1973).
- <sup>18</sup>R. L. Jaffe, M. D. Pattengill, and D. W. Schwenke, in *Supercomputer Algorithms for Reactivity. Dynamics and Kinetics of Small Molecules*, edited by A. Laganà (Kluwer, Dordrecht, 1989), p. 367.
- <sup>19</sup>S. P. Walch and R. L. Jaffe, *J. Chem. Phys.* **86**, 6946 (1987).
- <sup>20</sup>D. G. Hopper, *J. Chem. Phys.* **80**, 4290 (1984).
- <sup>21</sup>K. P. Huber and G. Herzberg, *Molecular Spectra and Molecular Structure, Vol. 4, Constants of Diatomic Molecules* (Van Nostrand Reinhold, New York, 1979).
- <sup>22</sup>G. Herzberg, *Molecular Spectra and Molecular Structure, Vol. 3, Electronic Spectra and Electronic Structure of Polyatomic Molecules* (Van Nostrand Reinhold, New York, 1966).
- <sup>23</sup>S. Bashkin and J. O. Stoner, *Atomic Energy Levels and Goujian Diagrams* (North Holland, Amsterdam, 1975).
- <sup>24</sup>K. S. Sorbie and J. N. Murrell, *Mol. Phys.* **29**, 1378 (1975).
- <sup>25</sup>J. N. Murrell and K. S. Sorbie, *J. Chem. Soc. Faraday II* **70**, 1552 (1974).
- <sup>26</sup>J. N. Murrell, S. Carter, S. C. Farantos, P. Huxley, and A. C. J. Varandas, *Molecular Potential Energy Functions* (Wiley, London, 1984).
- <sup>27</sup>S. P. Walch and R. L. Jaffe, AIP document No. PAPS JCPA-86-6946-10.
- <sup>28</sup>A. Solé, R. Sayós, J. M. Lucas, M. González, X. Giménez, M. Albertí, and A. Aguilar, in *Studies in Physical and Theoretical Chemistry*, edited by R. Carbó (Elsevier, Amsterdam, 1989), Vol. 62, p. 535.
- <sup>29</sup>R. Sayós, M. González, and A. Aguilar, *Chem. Phys.* **141**, 401 (1990).
- <sup>30</sup>NAG Routine F04AEF, Mark 14, The Numerical Algorithms Group Ltd. (Wilkinson House, Oxford, 1990).
- <sup>31</sup>NAG Routine E04HFF, Mark 14, The Numerical Algorithms Group Ltd. (Wilkinson House, Oxford, 1990).
- <sup>32</sup>M. Gilibert, M. González, and R. Sayós (unpublished work).
- <sup>33</sup>M. González and R. Sayós (unpublished work).
- <sup>34</sup>D. G. Truhlar and R. Steckler, *Chem. Rev.* **87**, 217 (1987).
- <sup>35</sup>M. Gilibert, M. González, and R. Sayós (unpublished work).
- <sup>36</sup>M. González, A. Aguilar, and M. Gilibert, *Chem. Phys.* **131**, 335 (1989).
- <sup>37</sup>M. González, A. Aguilar, and M. Gilibert, *Chem. Phys.* **131**, 347 (1989).
- <sup>38</sup>M. González and R. Sayós, *Chem. Phys. Lett.* **164**, 643 (1989).
- <sup>39</sup>R. Sayós, M. González, and A. Aguilar, *Chem. Phys.* **98**, 409 (1985).
- <sup>40</sup>M. Gilibert, A. Aguilar, M. González, and R. Sayós (work in progress).
- <sup>41</sup>J. C. Polanyi, *Acc. Chem. Res.* **5**, 161 (1972).
- <sup>42</sup>M. D. Pattengill, R. N. Zare, and R. L. Jaffe, *J. Phys. Chem.* **91**, 5489 (1987).
- <sup>43</sup>R. D. Levine and R. B. Bernstein, *Molecular Reaction Dynamics and Chemical Reactivity* (Oxford University, New York, 1979).